Combining UAV Multispectral Imaging and PROSAIL Model to Estimate LAI of Potato at Plot Scale

Shuang Li [1], Yongxin Lin [1], Ping Zhu [1], Liping Jin [1,2], Chunsong Bian [1,*] and Jiangang Liu [1,*]

[1] State Key Laboratory of Vegetable Biobreeding, Institute of Vegetables and Flowers, Chinese Academy of Agricultural Sciences, Beijing 100081, China; shuanglimailbox@163.com (S.L.); linyongxin1554@163.com (Y.L.); zhuping9717@163.com (P.Z.); jinliping@caas.cn (L.J.)

[2] Inner Mongolia Academy of Science and Technology, Hohhot 010021, China

* Correspondence: bianchunsong@caas.cn (C.B.); liujiangang@caas.cn (J.L.)

Abstract: Accurate and rapid estimation of the leaf area index (LAI) is essential for assessing crop growth and nutritional status, guiding farm management, and providing valuable phenotyping data for plant breeding. Compared to the tedious and time-consuming manual measurements of the LAI, remote sensing has emerged as a valuable tool for rapid and accurate estimation of the LAI; however, the empirical inversion modeling methods face challenges of low efficiency for actual LAI measurements and poor model interpretability. The integration of radiative transfer models (RTMs) can overcome these problems to some extent. The aim of this study was to explore the potential of combining the PROSAIL model with high-resolution unmanned aerial vehicle (UAV) multispectral imaging to estimate the LAI across different growth stages at the plot scale. In this study, four inversion strategies for estimating the LAI were tested. Firstly, two types of lookup tables (LUTs) were built to estimate potato LAI of different varieties across different growth stages. Specifically, LUT1 was based on band reflectance, and LUT2 was based on vegetation index. Secondly, the hybrid models combining LUTs generated by PROSAIL and two machine learning algorithms (random forest (RF), Partial Least Squares Regression (PLSR)) are built to estimate potato LAI. The determination of coefficient (R^2) of models for estimating LAI by LUTs ranged from 0.24 to 0.64. The hybrid method that integrates UAV multispectral, PROSAIL, and machine learning significantly improved the accuracy of LAI estimation. Compared to the results based on LUT2, the hybrid model achieved higher accuracy with the R^2 of the inversion model improved by 30% to 263%. The LAI retrieval model using the PROSAIL model and PLSR achieved an R^2 as high as 0.87, while the R^2 using the RF algorithm ranged from 0.33 to 0.81. The proposed hybrid model, integrated with UAV multispectral data, PROSAIL, and PLSR can achieve approximate accuracy compared with the empirical inversion models, which can alleviate the labor-intensive process of handheld LAI measurements for building inversion models. Thus, the hybrid approach provides a feasible and efficient strategy for estimating the LAI of potato varieties across different growth stages at the plot scale.

Keywords: potato; leaf area index; UAV multispectral imaging; PROSAIL; phenotyping

1. Introduction

As the third largest food crop in the world, the potato industry plays a crucial role in global food security [1]. As a shallow-rooted tuber crop, the harvested organ of potato is the underground tuber. There is a significant covariance between canopy and tuber, making canopy growth assessment critical for assessing potato nutritional status and predicting yield. The leaf area index (LAI) is a crucial parameter that can be directly employed to depict the canopy structure [2]. It is closely related to the physiological functions of crops and the nutrient and water cycles within ecosystems. It has been shown that potato yield is positively correlated to the leaf area index to a certain extent [3]. Meanwhile, the LAI is

of great significance in characterizing the canopy structure of vegetation and the growth status of vegetation [4]. Since the 1960s, the LAI has been used to quantify the interception of light by vegetation, and the interactions between features and light form the basis for vegetation monitoring through remote sensing [5]. Consequently, the leaf area index plays a crucial role in the remote-sensing monitoring of vegetation. Accurate monitoring of the LAI is beneficial for enhancing production efficiency, understanding the growth dynamic differences in different regions, and predicting the yield of potatoes, etc. This important application can promote the sustainable development of the potato industry and bring greater economic and social benefits to agricultural production.

Traditional methods for determining the LAI have included direct measurement, the use of optical instruments such as the LAI-2000 [6], and point quadrat techniques [7]. These methods, which are suitable for point-like areas, become impractical and inefficient when scaled up due to their lack of representativeness and the extensive time and labor they require. In contrast, remote-sensing technology enables LAI estimation over broader temporal and spatial scales, facilitating the accurate and dynamic monitoring of vegetation status. This technology serves as an essential tool for high-throughput phenotypic analysis in precision agriculture and breeding contexts [8].

Presently, LAI inversion models that employ remote-sensing technology are developed through two main methodologies: empirical statistical modeling and physical inversion modeling using RTMs [9]. Empirical models rely on establishing regression relationships between spectral reflectance or vegetation indices and measured data. Machine learning (ML) algorithms are the most commonly used methods for empirical modeling. ML not only trains models to automatically recognize and analyze spectral data—thereby improving the accuracy and generalization of LAI estimation—but also integrates data from different sensors and spectral bands for multidimensional analysis, providing a more comprehensive understanding of crop canopy characteristics and further enhancing LAI estimation accuracy. However, this approach can be significantly influenced by factors such as growth stage, ecological zone, and sensor type, which limits its applicability across different crops or varieties [10]. RTM-based models use physical laws to elucidate the causal relationships between plant components and radiation photon interactions, considering factors like crop canopy structure, growth status, and environmental conditions. The inversion of physiological indices based on RTMs is typically achieved through lookup tables and numerical optimization but both methods require substantial computational effort [11], limiting their use in hyperspectral scenarios. However, the hybrid inversion method, which combines RTMs with ML algorithms, capitalizes on the strengths of both approaches [12].

As a commonly used RTM, the PROSAIL model comprehensively accounts for the optical properties of soil and the geometric characteristics of vegetation [8,9]. It includes both forward simulation and inverse retrieval processes. By changing the input parameter values, the model simulates a large amount of hyperspectral data in the range of 400–2500 nm, completing the spectral forward simulation. Subsequently, it combines lookup tables or machine learning algorithms to estimate vegetation physiological and biochemical indices. The PROSAIL model is currently used in the inversion of various indices, such as the LAI, leaf chlorophyll content, canopy chlorophyll content, and canopy water content [13–16]. Research has shown that during the inversion of the LAI, optical remote-sensing signals can interfere with the optical features associated with chlorophyll content, leading to uncertainty in the inversion results of these two agronomic parameters [17]. Researchers have defined the red-edge position based on the abrupt changes in the reflectance curve between 680 and 750 nm. Reflectance at this position primarily arises from multiple reflections between the leaf layers and chlorophyll absorption [18]. Sun et al. have incorporated red-edge reflectance into the construction of vegetation indices, effectively improving the accuracy of crop LAI estimation [15].

The combination of RTMs with hyperspectral or multispectral imaging provides an effective approach for monitoring plant physiological and biochemical characteristics. Previ-

ous RTM-based inversions of physiological indicators have primarily utilized hyperspectral and satellite multispectral data. The REGFLEC model, combined with SPOT satellite data, has been used to estimate the LAI and chlorophyll content (Cab) for a wide range of crops, such as maize, wheat, and soybean [19]. The PROSAIL model, in conjunction with canopy hyperspectral information, has also been used to estimate chlorophyll content in potato leaves [20]. Highly accurate inversions of the LAI and chlorophyll content can be obtained using the PROSAIL model when incorporating multi-source satellite data [21]. In recent years, unmanned aerial vehicles (UAVs) have been playing an increasingly significant role in crop phenotyping. Compared to satellite remote sensing, UAV remote sensing offers greater flexibility and higher spatial and temporal resolution, making it a crucial tool for monitoring crop growth in the field [8,9]. Duan et al. evaluated the applicability of the LAI inversion using UAV hyperspectral data combined with PROSAIL modeling, including for potatoes [22]. While hyperspectral equipment provides rich spectral data, multispectral sensors generate less spectral information, reducing computational demands and data redundancy; however, a downside is that they may lack some relevant spectral bands. In contrast, integrating UAV-based multispectral imaging with RTMs offers significant advantages in addressing these limitations. Nevertheless, there is still limited research on the precise estimation of potato LAI using UAV multispectral remote sensing and canopy radiative transfer modeling, particularly in breeding and field trial plots.

Therefore, the objective of this study was to explore the potential of combining the PROSAIL model with UAV multispectral imaging to estimate potato LAI across key growing stages under different cultivars and nitrogen rates. Specifically, this study aimed to achieve the following: 1. Determine the sensitive model parameters of PROSAIL and the optimal lookup table size for potato LAI inversion. 2. Explore the potential of combining PROSAIL and UAV multispectral imaging for potato LAI inversion at plot scale. 3. Evaluate the performance of the hybrid method for estimating the LAI, compared to traditional empirical models based on the ground-truth measurements at different growth stages.

2. Materials and Methods

2.1. Experiment Design

The experiment was conducted in Chabei, Zhangjiakou, Hebei Province, China, in 2023 (Figure 1). This region is located in the temperate arid and semi-arid zone of East Asia's continental monsoon climate, with an altitude of 1390 m. The soil type is calcium chestnut. Two potato varieties, Zhongshu 5 and Zhongshu 49 (D681), were used in the experiment, along with five nitrogen fertilizer treatments (0, 50, 100, 250, and 400 kg·ha^{-1}), each with four replications. The crops were sown on 5 May and harvested on 8 September. Eight ground control points (GCPs) were placed around the experimental field, and the three-dimensional coordinates of the GCPs were determined using high-precision RTK GPS.

2.2. Data Acquisition

2.2.1. Remote-Sensing Data Acquisition and Pre-Processing

A DJI Inspire 2 (DJI Technology Co., Shenzhen, China) UAV equipped with a RedEdge-P multispectral camera (MicaSense, Seattle, WA, USA) was used as the remote-sensing platform (Figure 2). The spectral band information (Table 1) of the multispectral sensor is provided in Table 1.

In order to minimize the interference of background factors on the test results, the UAV was operated between 10:00 and 14:00. The flight altitude of the mounted multispectral sensor was 30 m, with both heading overlap and side-to-side overlap set at 75%. Calibration plates were photographed both before takeoff and after landing, and the images were radiometrically calibrated using a light sensor mounted on top of the UAV [8]. Multispectral image pre-processing (including radiometric and geometric correction) and image stitching (including alignment, optimizing alignment, generating dense point clouds, generating meshes, generating textures, generating digital elevation models, and digital

orthophotos) were performed using Agisoft Metashape Professional 2.0.2 software. ArcMap 10.8 software was used to realize image segmentation, and PyCharm Community Edition 2023.2.3 software was used to complete image background removal and spectral reflectance extraction in each band.
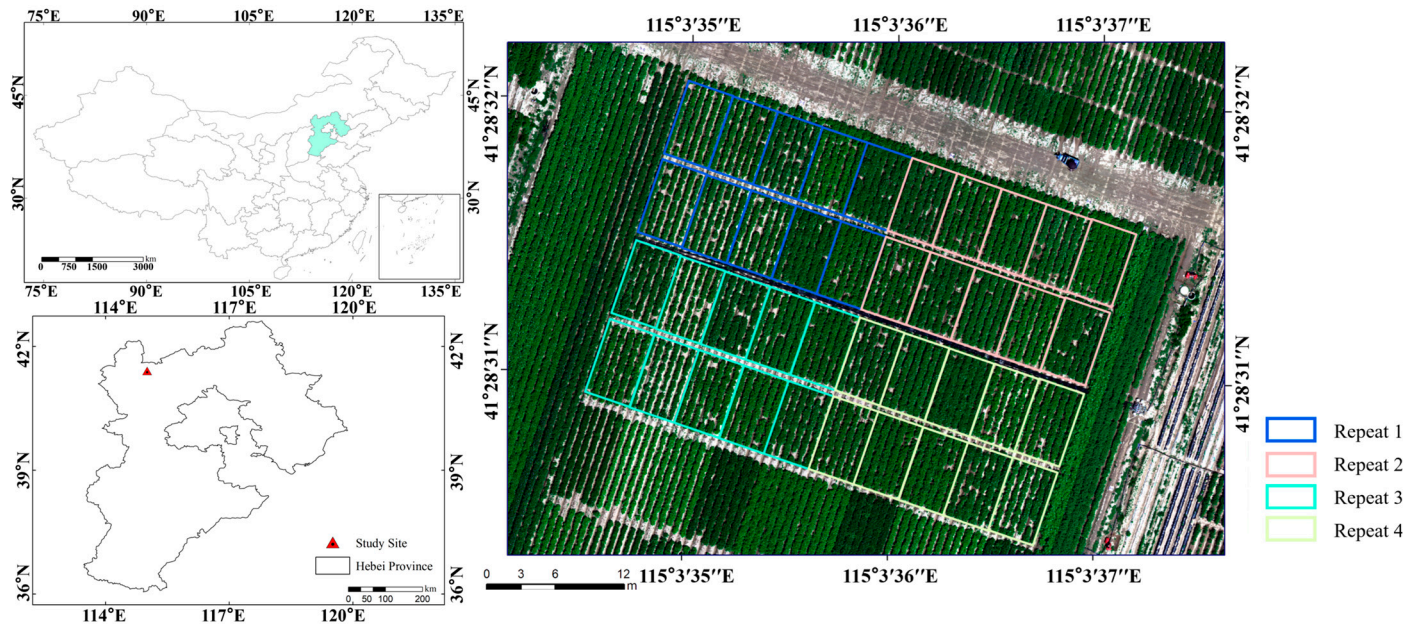
Figure 1. Location of the study area and field plot distribution.

Figure 2. Unmanned aerial vehicle multispectral image acquisition system.

Table 1. Spectral characterization of the MicaSense RedEdge-P camera for multispectral image acquisition.

Bands	Center Bands	Bandwidth	Resolution	Field of View
Blue	475 nm	32 nm	1456 × 1088 (1.58 MP per multispectral band)	49.6° × 38.3° VFOV
Green	560 nm	27 nm	1456 × 1088 (1.58 MP per multispectral band)	49.6° × 38.3° VFOV
Red	668 nm	16 nm	1456 × 1088 (1.58 MP per multispectral band)	49.6° × 38.3° VFOV
Red-edge	717 nm	12 nm	1456 × 1088 (1.58 MP per multispectral band)	49.6° × 38.3° VFOV
Near-infrared	842 nm	57 nm	1456 × 1088 (1.58 MP per multispectral band)	49.6° × 38.3° VFO
Panchromatic	634.5 nm	463 nm	2464 × 2056 (5.1 MP panchromatic band)	44.5° × 37.7° VFOV

The spectral response function (SRF) for each band was calculated based on the transmittance of the respective band filter of the RedEdge-P multispectral sensor. Simulated spectral reflectance was then resampled to the center wavelength of the RedEdge-P sensor according to the SRF (Figure 3), in order to construct the equivalent spectral reflectance of

the simulated band information. The equivalent spectral reflectance based on the RedEdge-P spectral response function is calculated as follows [23]:

$$R_{rs}(band_i) = \frac{\int_{\lambda_1}^{\lambda_2} R_{rs}(\lambda) SRF(\lambda) d(\lambda)}{\int_{\lambda_1}^{\lambda_2} SRF(\lambda) d(\lambda)} \tag{1}$$

where $R_{rs}(band_i)$ is the equivalent spectral reflectance in $band_i$ of the sensor; λ_1 and λ_2 are the band range of the band; $R_{rs}(\lambda)$ is the simulated optical reflectance; and $SRF(\lambda)$ is the spectral responsivity at λ wavelength.
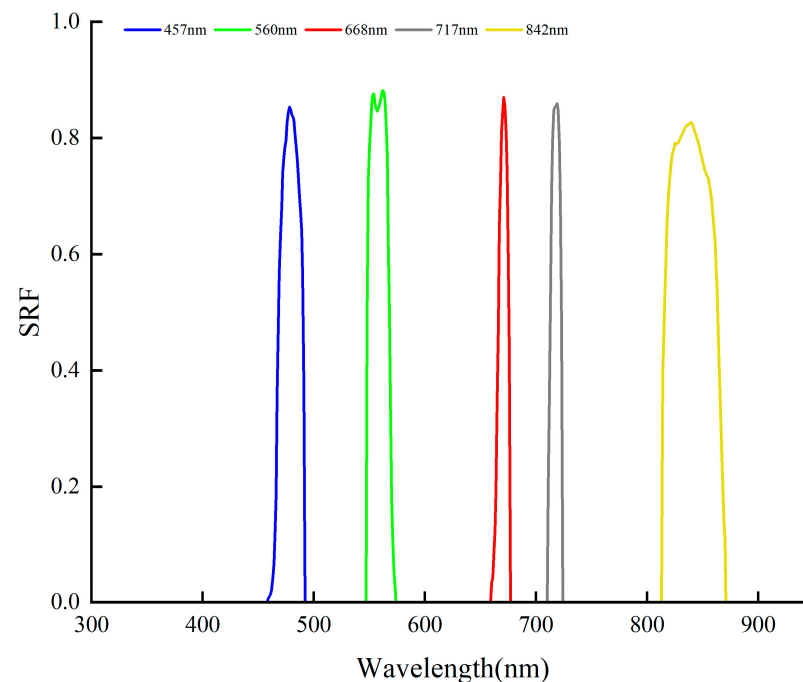
Figure 3. Spectral response function of the RedEdge-P multispectral sensor used.

2.2.2. Agronomic Data Acquisition

A total of four plant canopy biomass collections were completed across 40 plots during the potato tuber initiation and tuber bulking stages. Simultaneously, data on the leaf area index, equivalent water thickness, chlorophyll content, and carotenoid content were also collected (Table 2).

Table 2. Overview of agronomic data acquisition.

Growth STAGE	Time	Number of Subdivisions (Number)	Parameter
Tuber initiation stage	4 July 2023	80	Biomass, LAI, chlorophyll content, carotenoid content, equivalent water thickness
Tuber initiation stage	15 July 2023	80	Biomass, LAI, equivalent water thickness
Tuber bulking stage	3 August 2023	80	Biomass, LAI, chlorophyll content, carotenoid content, equivalent water thickness
Tuber bulking stage	14 August 2023	80	Biomass, LAI, chlorophyll content, carotenoid content, equivalent water thickness

Six plants were collected from each plot. The leaves, stems, roots, underground stems (excluding the tuber), and tubers were separated. The leaves were then killed at 105 °C for 30 min, followed by drying at 85 °C until the biomass reached a constant weight. Afterward, the dry matter weight was measured. Dry matter content ($g \cdot cm^{-2}$) was calculated as the

above-ground biomass per unit area. Before weighing the fresh weight of the samples, leaf images were captured using a camera. Leaf image extraction was then performed by separating the plant from the background through threshold segmentation (Figure 4). The leaf area index was derived from the pixel occupancy of the leaf area. Equivalent water thickness and dry matter content were calculated from the measured leaf area, dry weight, and fresh weight. During the same period, three plants were selected from each plot, and four leaves from each plant were brought back to the laboratory. Each leaf sample, with an area of 2.5 cm^2, was weighed to 0.1 g. The samples were then immersed in 96% ethanol until the material turned white. Absorbance measurements were taken with a UV spectrophotometer at 470, 649, and 665 nm wavelengths. These measurements were used to calculate the chlorophyll and carotenoid content (in mg/g) by combining the absorbance data with the mass of the samples. The calculation formula is as follows:

$$C_a = 13.95D_{665} - 6.88D_{649} \tag{2}$$

$$C_b = 24.96D_{649} - 7.32D_{665} \tag{3}$$

$$C_{x,c} = \frac{1000D_{470} - 2.05C_a - 114.8C_b}{245} \tag{4}$$

$$C_{ab} = \frac{(C_a + C_b) \times V \times N}{1000 \times S} \tag{5}$$

$$C_{ar} = \frac{C_{x,c} \times V \times N}{1000 \times S} \tag{6}$$

where C_a and C_b are the concentrations of chlorophyll a and chlorophyll *b* (mg·L^{-1});

Figure 4. Leaf area photo background removal effect.

$C_{x,c}$ is the concentration of carotenoids (mg·L^{-1});
C_{ab} is the chlorophyll content (µg·cm^{-2});
Car is the carotenoid content (µg·cm^{-2});
D_{665}, D_{649}, and D_{470} represent the extinction of chloroplast pigment extracts at wavelengths of 665 nm, 649 nm, and 470 nm;
V is the total volume of the extract (mL); *N* is the dilution factor; *S* is the leaf area (cm^2).

2.3. PROSAIL Model

The PROSAIL model, which integrates the leaf radiative transfer model PROSPECT and the canopy radiative transfer model SAIL, is the most commonly used RTM for simulating crop canopy reflectance as a function of the LAI, leaf angle distribution function, chlorophyll content, dry matter content, carotenoid content, leaf equivalent water thickness, canopy reflectance background, sensor viewing angle, sun zenith, and azimuth angles [9]. The PROSPECT-5 and 4SAIL models (http://teledetection.ipgp.jussieu.fr/prosail/, accessed on 30 September 2024) were used in this study. The PROSPECT model assumes the

leaf blade structure as a multilayer flat plate with a rough surface. It also assumes that light rays are both isotropic and parallel, and simulates Lambertian scattering of light rays between the flat plates by inputting the physical and chemical parameters of the leaves. This results in the calculation of the leaf reflectance and transmittance over the 400 to 2500 nm spectral range. The leaf spectral information simulated by the PROSPECT model is then used as input for the SAIL model. The SAIL model assumes that the vegetation canopy is a homogeneous, infinitely extensible mixed medium with isotropic leaves. It simulates the radiative transfer process within the canopy using radiative transfer equations as the theoretical basis to obtain the canopy-scale reflectance. There are two commonly used inversion methods for radiative transfer modeling, the LUT-based method and the hybrid inversion method that combines machine learning [20]. Due to the "same effect with different parameters" problem in RTM inversion, combining sensitivity analysis results, a priori knowledge, and measured data can effectively reduce the occurrence of this phenomenon—where different parameters lead to the same spectral response [14].

2.3.1. Sensitivity Analysis

Sensitivity analysis is an important method for qualitatively and quantitatively assessing how changes in model parameters affect the model's output. By combining measured data with a priori knowledge, the ranges and fixed values for model parameters used in sensitivity analysis are determined. Based on the results of this analysis, the input parameter ranges and fixed values for constructing the final lookup table are established.

A local sensitivity analysis of the 14 model parameters was conducted, treating each parameter individually as a variable while fixing the others. This analysis qualitatively evaluated how the input parameter ranges influenced the reflectance in the desired spectral band. The sensitive model parameters were identified from the local sensitivity analysis, and a global sensitivity analysis was then performed on these parameters using the Sobol method to quantitatively assess how changes in the model parameters impact the model's output. The ranges of the sensitivity analysis parameters and the settings for fixed values are presented in Appendix A Table A1.

2.3.2. Lookup Tables (LUTs)

In PROSAIL model inversion, the number of parameters determined by a priori knowledge or fixed values is typically much larger than the number of field-obtained parameters within the setup range. This discrepancy makes it difficult for radiative transfer models to directly invert the desired vegetation growth parameters based solely on spectral information; however, LUTs provide a solution to this issue [24]. With the LUT-based inversion method, the optimal combination of parameters corresponding to the simulated spectrum that most closely matches the measured spectrum can be identified through a simple search process. In this study, the LAI was retrieved at two stages—the tuber initiation stage and the tuber bulking stage—for both the late-maturing variety D681 and the early-maturing variety Zhongshu 5. The simulated spectral reflectance of the PROSAIL model was combined with the spectral response function of the RedEdge-P sensor to calculate the equivalent spectral reflectance, which is referred to as the simulated spectral reflectance. Two types of lookup tables were constructed: LUT1, which was based on five bands of simulated spectral reflectance; and LUT2, which contained six simulated vegetation indices derived from five bands of simulated spectral reflectance (see Table 3).

Table 3. Vegetation index used in this study.

Name	Formulas	References
Optimized soil-adjusted vegetation index (OSAVI)	$(1 + 0.16)\frac{NIR-R}{NIR+R+0.16}$	[25]
Red-Edge Normalized Difference Vegetation Index (NDVIre)	$\frac{\rho_{RE}-\rho_{Red}}{\rho_{RE}+\rho_{Red}} \times \rho_{NIR}$	[15]
Red-Edge Modified Simple Ratio (MSRre)	$\frac{\rho_{RE}/\rho_{Red}-1}{\sqrt{\rho_{RE}/\rho_{Red}+1}} \times \rho_{NIR}$	[15]
Soil-adjusted vegetation index (SAVI)	$(1 + 0.5)\frac{(NIR-R)}{(NIR+R+0.5)}$	[26]
Enhanced Vegetation Index (EVI)	$2.5\frac{NIR-R}{(NIR+6R-7.5B)+1}$	[27]
Modified Triangular Vegetation Index 2 (MTVI2)	$1.5\frac{(1.2(NIR-G)-2.5(R-G))}{\sqrt{(2NIR+1)^2-(6NIR-5\sqrt{R})-0.5}}$	[28]

In the LUT-based inversion, the LAI was estimated when the root mean square error (*RMSE*) and mean absolute error (*MAE*) between the UAV-measured values and the simulated spectra in the lookup table were minimized, based on the cost function. The parameter combination with the smallest mean *RMSE* and *MAE* was then chosen as the inversion result.

The cost function used to establish the relationship between the measured spectra (or vegetation indices) and the modeled spectra (or vegetation indices) is defined as follows:

$$RMSE = \sqrt{\frac{1}{n}\sum(R_{simulated} - R_{measured})^2} \tag{7}$$

$$MAE = \frac{1}{n}\sum_{i=1}^{n}|R_{simulated} - R_{measured}| \tag{8}$$

where *n* is the number of bands or vegetation indices; $R_{simulated}$ is the simulated reflectance value or vegetation index constructed by simulated reflectance; $R_{measured}$ is the measured band reflectance value or vegetation index constructed by measured reflectance.

To minimize the impact of lookup table size on the final inversion results, the full-life data for the two varieties were used as examples for pre-inversion lookups based on the distribution ranges of the model parameters provided in Appendix A Table A2. Lookup tables containing 1000, 5000, 10,000, 20,000, and 50,000 simulated spectral reflectance were constructed using the Latin hypercube sampling method. The optimal lookup table size was determined by comparing the inversion results of LUT1, and the construction of each lookup table (LUT) was completed using this optimal size.

2.3.3. Machine Learning Algorithms

RF and PLSR are widely used to estimate potato LAI, demonstrating strong performance in previous research. This study emphasizes the potential of empirical statistical modeling and radiation modeling methods in estimating potato leaf area index at the community scale, thus, RF and PLSR were chosen.

Random Forest Algorithm

The random forest (RF) algorithm introduces the concept of bagging, which involves constructing a series of unrelated decision trees by randomly selecting samples and features [29]. In addition, during the construction of each decision tree, each node randomly selects a subset of features and chooses the optimal features for splitting. The model demonstrates good predictive ability, high tolerance to noise and outliers, and can avoid overfitting to some extent. Each decision tree makes predictions based on the selected samples and features. By averaging the regression predictions of all decision trees, the overall regression prediction for the forest is obtained. Training the RF model requires setting several parameters, including the number of trees, the number of random features, and the stopping criterion. The RF model is built using the scikit-learn library in Python,

and the entire process is carried out in PyCharm Community Edition 2023.2.3. The number of decision trees is set to 100, and the number of features is determined by the square root of the total number of features. The training process stops when the minimum number of samples in the tree nodes is one, and the minimum impurity is zero.

Partial Least Squares Regression Algorithm

Partial Least Squares Regression (PLSR) is a statistical method for modeling linear regression between multivariate data. PLSR is able to handle multiple response variables simultaneously and can effectively solve the multicollinearity problem by finding the direction that explains the maximum covariance between the independent and dependent variables to reduce the dimensionality of the data and construct predictive models [30]. PLSR model construction and validation were accomplished by loading the pls package using the R version 4.2.2 language.

The equivalent spectral reflectance was used to construct the vegetation index; the simulated vegetation index and the corresponding parameter input range were used as the modeling set; and the measured data were used as the validation set. The machine learning algorithm was combined to realize the potato LAI inversion based on the simulated data.

Hybrid Modeling Strategy

Using LUT2 simulation data as the modeling set, and RMSE and MAE as the cost functions, we screened out the lookup table information with the smallest mean values of RMSE and MAE compared to the UAV multispectral vegetation index. We combined the spectral index with RF and PLSR algorithms to construct hybrid inversion models. The field-measured LAI in 2023 was used as the validation set. The inversion model constructed using PROSAIL simulated spectral data and the machine learning algorithm with the field-measured LAI were compared to verify the feasibility of the hybrid modeling method for estimating potato LAI.

2.4. Model Evaluation and Statistical Analysis

The inversion of the LAI during the tuber initiation stage and tuber bulking stage, for two varieties, as well as the comprehensive LAI inversion for the entire growth period of the two varieties, was achieved using simulated spectral data and input model parameter ranges. The inversion accuracy was validated using actual measured multispectral data from UAV and ground-truth data. The model performance was evaluated using two statistical indicators: the coefficient of determination (R^2) and *RMSE*. The formulas for the evaluation criteria are as follows:

$$R^2 = 1 - \frac{\sum_{i=1}^{m} (\hat{y}_i - \overline{y})^2}{\sum_{i=1}^{m} (y_i - \overline{y})^2} \tag{9}$$

$$RMSE = \sqrt{\frac{1}{m} \sum_{i=1}^{m} (y_i - \hat{y}_i)^2} \tag{10}$$

where yi represents the observed LAI values; $\overline{y}$ represents the mean of the observed LAI values; $\hat{y}_i$ represents the predicted LAI values; and m represents the number of prediction points.

3. Results
3.1. Sensitivity Analysis of the PROSAIL Model Parameters
3.1.1. Local Sensitivity Analysis

In order to localize the parameters of the PROSAIL model, the numerical range and fixed value are determined based on the measured data and prior knowledge during sensitivity analysis. As shown in Figure 5, when the LAI is less than 3 and when the LAI is between 3 and 6, it exhibits a varying impact on the spectral reflectance response in the

400 nm to 2500 nm bands. Specifically, an increase in the LAI is associated with an increase in reflectance in the visible, red-edge, and near-infrared regions, with the effect being more pronounced when the LAI is less than three. Chlorophyll content (Cab) significantly affects the reflectance in the visible and red-edge bands, with reflectance in the visible region decreasing as chlorophyll content increases. Carotenoid content (Car) only influences reflectance in the visible band. The dry matter content (cm) affects reflectance in the 780 nm to 2500 nm range, in addition to the visible spectrum. Water content (Cw) notably affects reflectance between 860 nm and 2500 nm. The presence of brown matter (Cbrown) alters reflectance in both the visible and near-infrared (NIR) spectra. Leaf area (ALA), nitrogen content (N), and hotspot factor (hspot) significantly affect reflectance between 760 nm and 2400 nm. Reflectance decreases with increasing ALA but increases with higher N and hspot values. Sky reflectance (Skyl), soil reflectance (psoil), and leaf thickness (tts) mainly influence the NIR spectrum up to 1000 nm, with minimal impact on reflectance fluctuations. The value of leaf thickness (tto) affects reflectance across the full spectral range but has little effect on the visible spectrum. Since the tto is not the main focus of this study, a value of 0 is used as the standard in model construction. Finally, the parameter psi has no significant effect on reflectance across the full band range.

The analysis shows that the LAI, ALA, hspot, N, Cab, Car, Cm, Cbrown, and Cw have a significant effect on reflectance in the visible and red-edge bands. Although Cbrown also influences reflectance at wavelengths shorter than 1000 nm, the actual measurement data for Cbrown are unavailable. Based on previous studies, Cbrown is set to a constant value of 0 when constructing the lookup table. The parameters psoil, skyl, ts, to, and psi have negligible effects on reflectance; therefore, they are set to constant values of 0 during the global sensitivity analysis.

3.1.2. Global Sensitivity Analysis

The results of the local sensitivity analysis showed that the spectral response in the visible region varied with the LAI value. The global sensitivity analysis is discussed in terms of 0 < LAI < 3 and 3 < LAI < 6, respectively. The global sensitivity analysis shows that when the LAI < 3, the reflectance at the bands shown in Table 1 is mostly affected by the LAI, and that 842 nm is mainly affected by Cm (69.16%). The percentage of LAI effect on canopy reflectance at 475 nm, 560 nm, 668 nm, and 717 nm was 99.79%, 94.93%, 99.58%, and 74.62%, respectively. When the LAI > 3, the inverse at the bands shown in Table 1 is mainly affected by the LAI, ALA, and Cab, and at 842 nm, it is still mainly affected by Cm (73.14%). The canopy reflectance at 475 nm was mainly affected by ALA (83.64%), followed by the LAI (9.83%). The 560 nm canopy reflectance was mainly affected by the Cab (76.66%). The spectral reflectance at 668 nm is affected by ALA, LAI, Cab, and hspot in the order of 37.23%, 31.18%, 15.67%, and 14.07%, respectively, and the spectral reflectance at 717 nm is mainly affected by the Cab, which affects the results by 60.73% (Figure 6). The results showed that the canopy structural parameters and chlorophyll content had a great influence on the visible light and near-infrared reflectance during the vigorous shoot growth stage, and it was very important to understand and reduce the influence of chlorophyll content on reflectance in the LAI retrieval.

3.2. Effect of Lookup Table Size on Inversion Results

With the increase in the number of simulated spectra included in the lookup table, the accuracy of the LAI inversion model based on PROSAIL improves (Figure 7); however, when the number of simulated spectra exceeds 10,000, the time required to construct the LUTs increases significantly, while the accuracy of the LAI inversion model starts to decrease. Figure 7 shows that the construction times for LUTs containing 1000, 5000, 10,000, 20,000, and 50,000 spectral data took 88.577 s, 440.864 s, 889.426 s, 1761.24 s, and 4568.293 s, respectively. Using LUT1 with 1000 simulated data, the modeling R^2 is 0.28 and RMSE is 1.81. When the simulated spectral data in LUT1 increased to 10,000, R^2 increased by 89.82% and the RMSE reduced by 57.51%. In addition, when the simulated spectra in

the LUT exceeded 10,000 and continued to increase, the accuracy of the LAI inversion model decreased. This may be due to the larger lookup table amplifying the effects of the phenomenon where "different parameters have the same spectral reflectance" on the model results. Based on the above results, LAI retrieval was conducted using the LUT containing 10,000 simulated spectra.
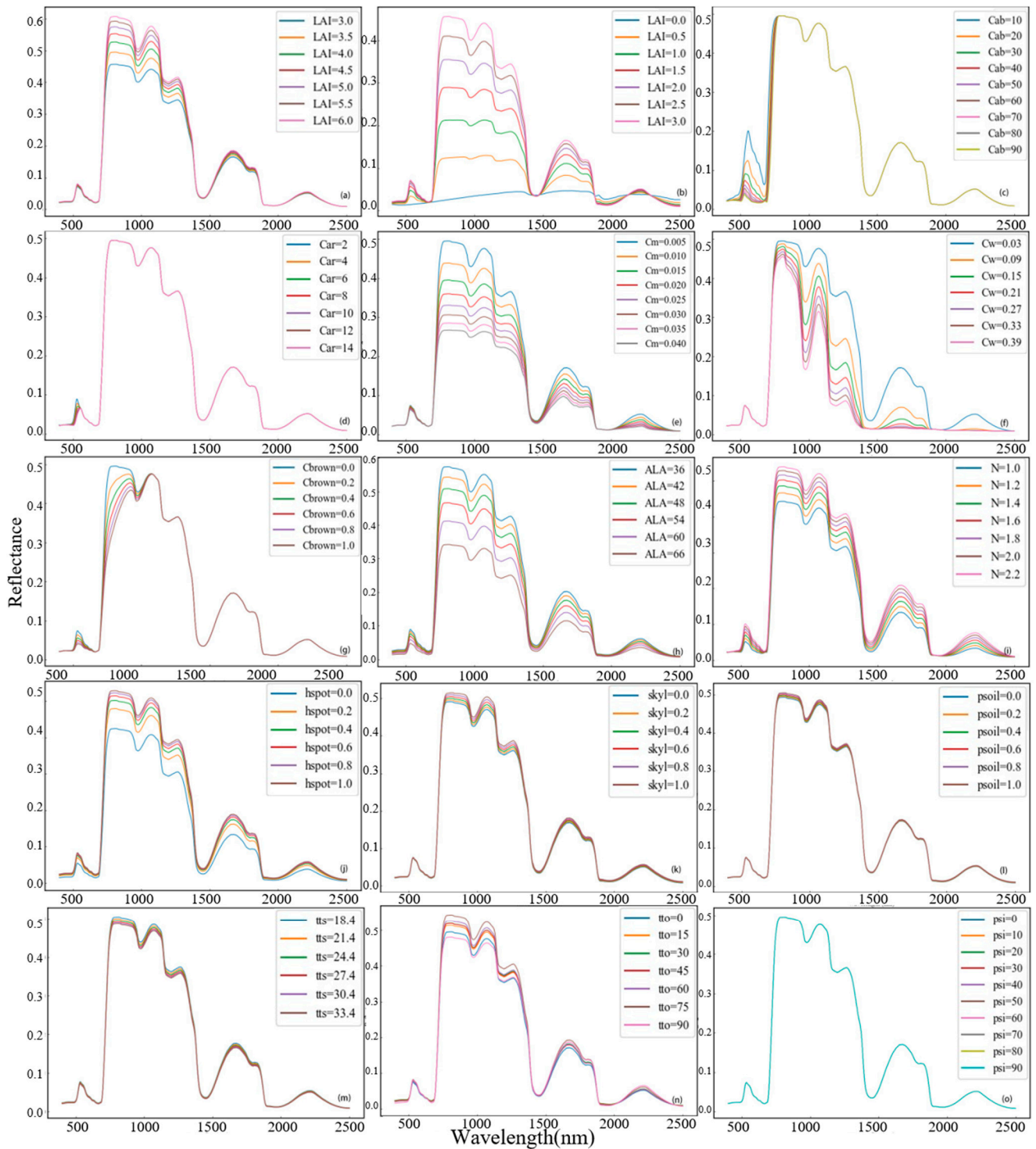
Figure 5. Local sensitivity analysis of PROSAIL model parameters. Figures (**a**,**b**) show the variation in spectral reflectance at 400–2500 nm for 3 < LAI < 6 and 0 < LAI < 3; (**c**–**o**) show the effects of Cab, Car, Cm, Cw, Cbrown, hspot, ALA, N, skyl, psoil, tts, tto, and psi on the spectral reflectance at 400 nm–2500 nm, respectively.
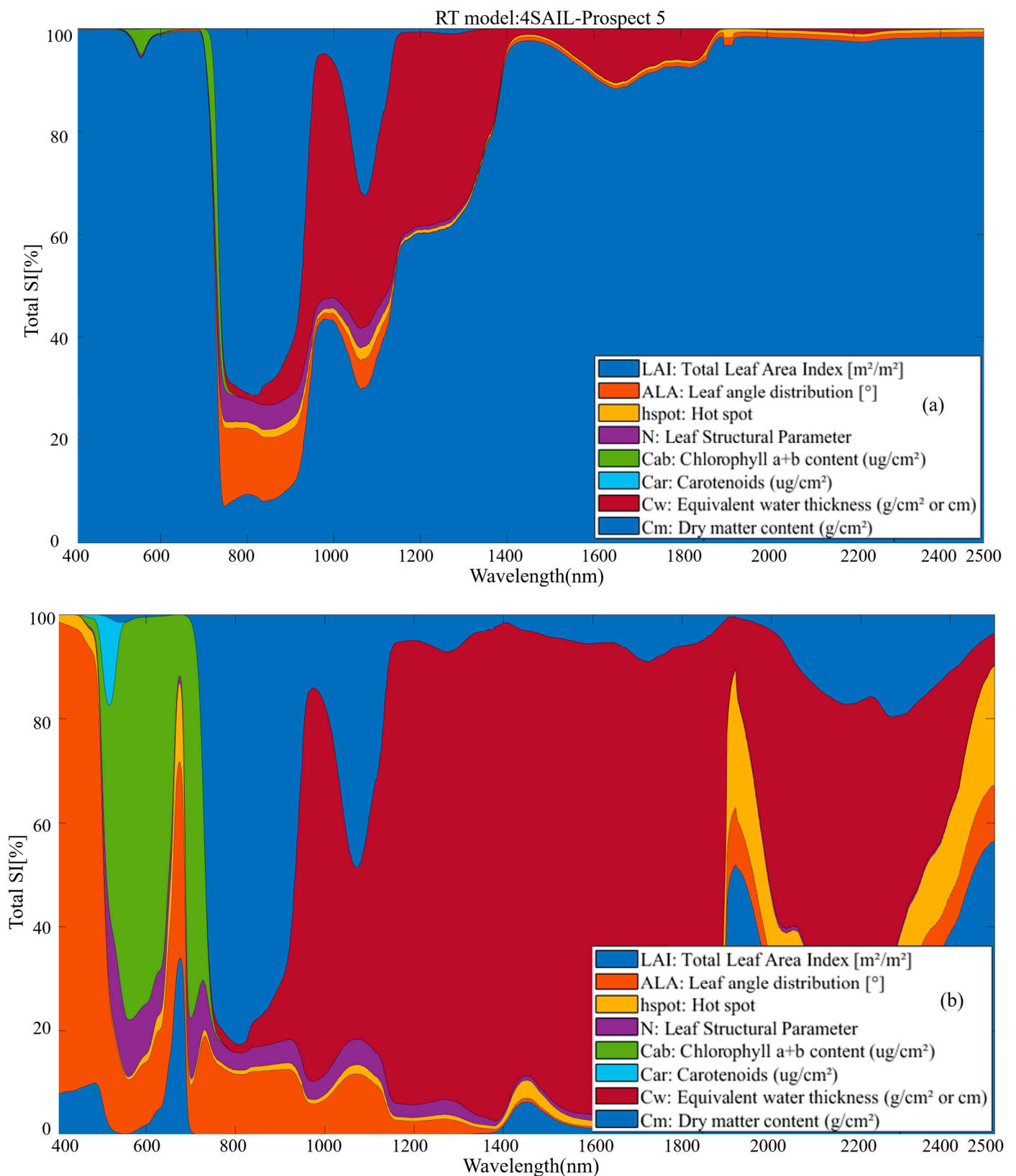
Figure 6. Global sensitivity analysis of the main PROSAIL model parameters: (**a**) the result of global sensitivity analysis for 0 < LAI < 3; (**b**) the result of global sensitivity analysis for 3 < LAI < 6.
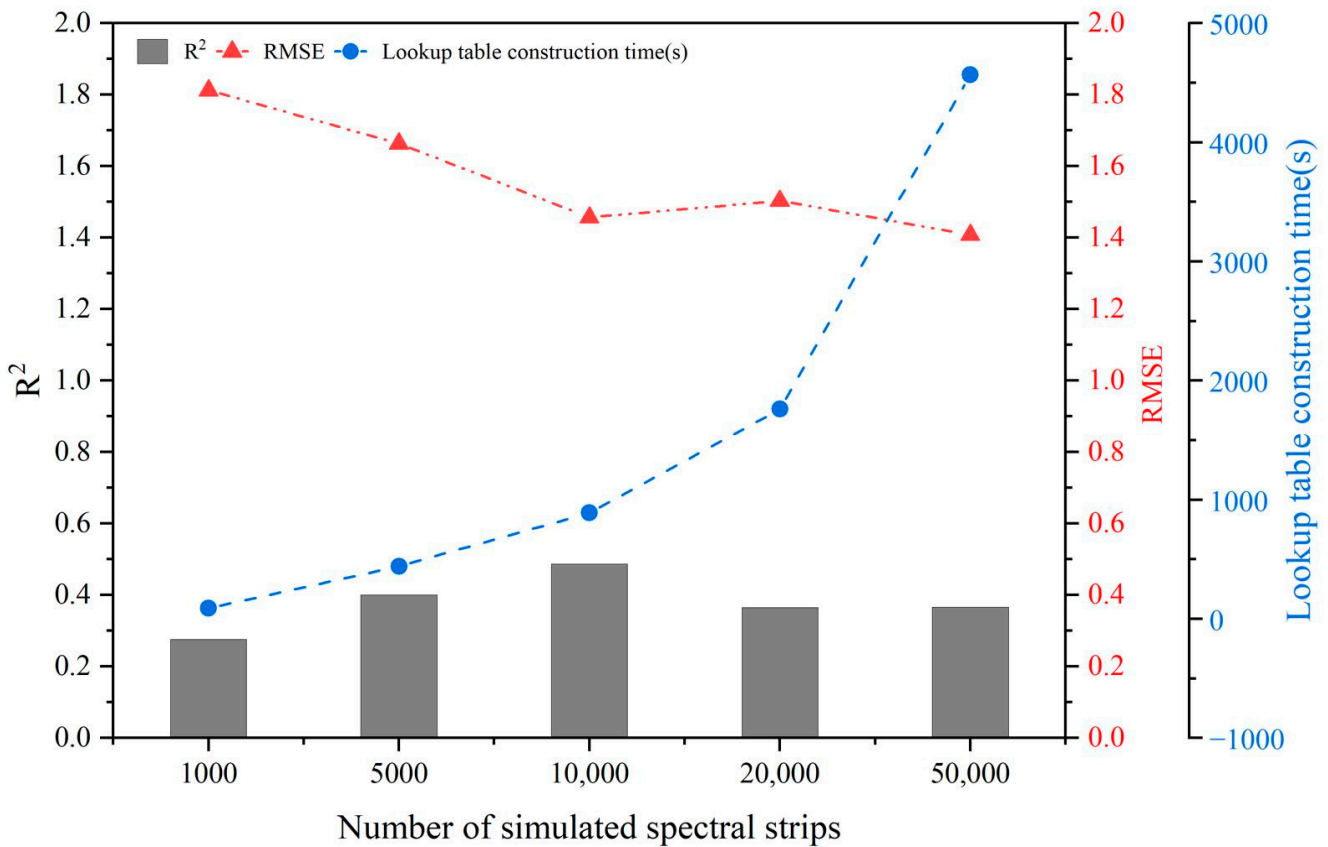
Figure 7. Results of LAI inversion using LUT1.

3.3. Potato LAI Inversion Based on Different Methods

The results of potato LAI inversion based on the PROSAIL model are shown in Table 4 and Figure 8; the hybrid inversion method using the PROSAIL model combined with the machine learning algorithm significantly improves the accuracy of model inversion. The accuracy of LAI inversion using LUT1 was stable for each growth stage and each variety, while LUT2 had a poor inversion effect for the tuber bulking stage. However, except for the tuber bulking stage, the inversion results based on LUT2 were better than LUT1 at each stage. The modeling accuracy of the hybrid inversion method based on LUT2 is significantly higher than that of the previous two methods. Except for the tuber bulking stage, the validation R^2 of the hybrid model of PROSAIL and RF is between 0.53 and 0.81 but the validation R^2 of this modeling method for the tuber bulking stage is only 0.33. The inversion accuracy of the hybrid model of PROSAIL combined with PLSR at each stage of the growth periods of potato is generally good, and the R^2 of the LAI verification at each stage and for both varieties based on this method is 0.67–0.88, and RMSE is 0.28–1.18. Compared with the inversion results using LUT2, the model R^2 of the tuber initiation stage, the tuber bulking stage, D681, Zhongshu5, and the whole growth stage increased by 30%, 263%, 49%, 47%, and 47%, respectively. The hybrid modeling method of PROSAIL + PLSR solves the problem of the low modeling accuracy and overfitting of PROSAIL + RF in the tuber expansion stage, significantly improves the accuracy of the LAI inversion model, and improves the stability of the LAI inversion model in different periods and varieties.

Table 4. Inversion of LAI results based on LUT1, LUT2, and hybrid methods.

| Modeling Period/Species | LUT1 | | LUT2 | | PROSAIL + RF | | | | PROSAIL + PLSR | | | |
| | | | | | Modeling Set | | Validation Set | | Modeling Set | | Validation Set | |
	R^2	RMSE	R^2	RMSE	R^2	RMSE	R^2	RMSE	R^2	RMSE	R^2	RMSE
M1	0.42	0.25	0.64	0.56	0.96	0.12	0.81	0.51	0.76	0.30	0.83	0.46
M2	0.43	1.24	0.24	1.80	0.90	0.49	0.33	1.66	0.56	0.85	0.87	1.18
D681	0.56	0.80	0.45	1.23	0.93	0.33	0.53	1.07	0.73	0.64	0.67	0.89
Z5	0.56	0.37	0.60	0.56	0.92	0.20	0.74	0.47	0.74	0.35	0.88	0.28
ALL	0.52	0.77	0.51	1.06	0.93	0.28	0.60	0.94	0.70	0.56	0.75	0.80

Note: M1, M2, Z5, and ALL represent all data during tuber initiation stage, tuber bulking stage, for zhongshu5, and for the full-life span of the two varieties, respectively.
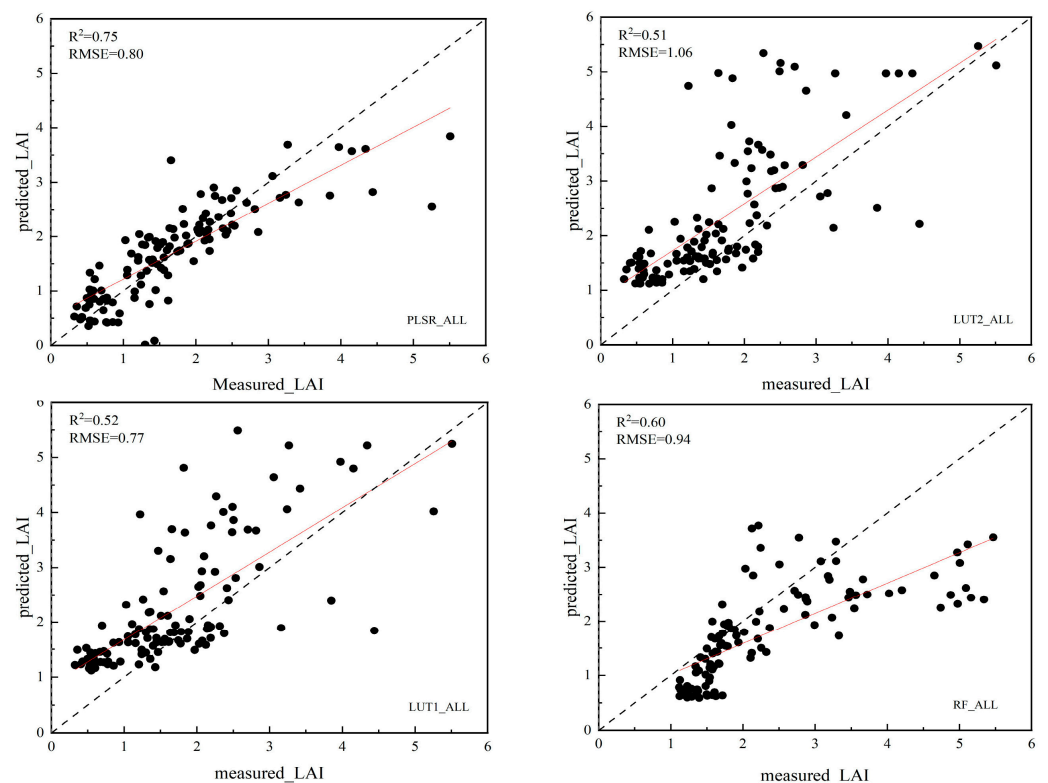
Figure 8. LAI inversion results of potato varieties across all growth stages using four strategies. The above results are for the model validation set, and the hybrid model results are for model validation using measured data.

3.4. Comparison of LAI Inversion Results Based on PROSAIL and Empirical Modeling

The LAI inversion results for each stage or variety based on field-measured data showed that the validation R^2 of the RF model for the LAI estimation across five stages or varieties ranged from 0.41 to 0.80 (Table 5). The model using the PLSR algorithm for the LAI inversion was more stable than those of RF, and the LAI inversion result was the best for the different stages or varieties, with the R^2 of the model verification ranging from 0.57 to 0.94.

Table 5. Empirical modeling results based on measured data.

Modeling Period/Species	RF				PLSR			
	Modeling Set		Validation Set		Modeling Set		Validation Set	
	R^2	RMSE	R^2	RMSE	R^2	RMSE	R^2	RMSE
M1	0.84	0.24	0.75	0.29	0.79	0.28	0.69	0.31
M2	0.76	0.51	0.65	0.55	0.79	0.63	0.57	0.79
D681	0.70	0.53	0.41	0.65	0.85	0.35	0.73	0.58
Z5	0.90	0.14	0.80	0.19	0.92	0.15	0.94	0.12
ALL	0.79	0.36	0.63	0.48	0.72	0.45	0.70	0.71

Note: M1, M2, Z5, and ALL represent all data during tuber initiation stage, tuber bulking stage, for zhongshu5, and for the full-life span of the two varieties, respectively.

These results indicate that the proposed hybrid inversion method, which combines potato simulation data with the empirical model based on measured data, achieves excellent accuracy. Moreover, the simulated data modeling approach requires only a small number of measured samples to define the range of the LAI indicators and verify the model. This can effectively reduce the challenges in constructing the inversion model, especially in cases where there is a low measured sample size or difficulties with measurements in large-scale scenarios.

4. Discussion

4.1. Performance of Inversion Models for Potato LAI Estimation

The combination of multispectral data and the PROSAIL model can accurately estimate the LAI at different growth stages and for different potato varieties, avoiding the problems of limited feasibility and model instability caused by small or insufficient sample sizes in a single growth stage. Spectral indices usually exhibit insensitivity at earlier growth stages, and saturation at later growth stages [25,26]. When using optical imaging to invert the leaf area index, it is prone to saturation in areas with high LAI, resulting in low inversion accuracy [31]. In the inversion results using lookup tables and PROSAIL combined with RF, the lower accuracy of the tuber bulking stage may be due to spectral saturation at large LAI values—which reduces the sensitivity of reflectance in the visible, red-edge, and near-infrared bands to LAI changes—and the increased interference of indicators such as chlorophyll content and average leaf inclination on spectral reflectance. Future studies should aim to mitigate the influence of these factors on LAI retrieval results by optimizing parameters or introducing novel vegetation indices.

The observed LAI is necessary for the empirical inversion strategy, which must be collected with manually handled measurements. As we know, LAI measurements can be conducted using devices such as a Plant Canopy Analyzer (LAI-2000, LI-COR, Lincoln, NE, USA), AccuPAR LP-80 ceptometer (METER Group, Pullman, WA, USA), and LI-3100C leaf area meter (LI-COR, Lincoln, NE, USA), which is also time-consuming and labor-intensive at the plot scale [9,10]. The hybrid strategy proposed in this manuscript combines the PROSAIL model, high-resolution unmanned aerial vehicle multispectral imaging, and machine learning algorithms to estimate potato LAI at the plot scale, which can be estimated without observed LAI data collection. The accuracy of LAI estimation models by the hybrid method and empirical modeling was compared, which displayed that the hybrid method can provide a similar estimation accuracy compared to empirical modeling. The hybrid approach offers substantial practical benefits due to reduced labor demands, which can improve the LAI estimation efficiency at the plot scale.

The hybrid inversion method used in this study can be implemented based on simulated data, greatly reducing the dependence on field data and proposing a feasible method for large-scale estimation of potato LAI, which is worthy of further validation in a broader agricultural scenario. When using PROSAIL and RF to estimate potato LAI, there exists a sharp drop in the accuracy of the training and validation of models, with the R^2 dropping from 0.93 to 0.60. Both the modeling set and validation set were chosen by random sam-

pling, so this drop may be caused by overfitting of the RF model. This can be attributed to insufficient training datasets or overly complex training models [15,19,22]. Overfitting is a common problem in machine learning—while it performs well on the training set and poorly on the test data [10]. Building a random forest model using methods such as bagging and booting may be a potential strategy to improve the model's generalization ability [18]. Moreover, increasing the amount of datasets may be helpful for improving the LAI inversion accuracy using the random forest algorithm in future research. Moreover, the contribution of the model structures (e.g., different deep learning algorithms) to the LAI estimation can be explored with specific themes in the future.

4.2. Impact of Sensitive Parameter Determination on Model Results

Sensitivity analysis revealed that canopy reflectance is predominantly influenced by ALA and Cab when the LAI exceeds three, corroborating results from previous studies [14].

External factors such as weather conditions [32], remote-sensing data acquisition angle [23], and brown pigment content [33] at the time of image acquisition have a great impact on LAI estimation. This suggests that differentiating between cloudy and clear weather conditions [34,35] can enhance inversion accuracy for high LAI values. However, this study's scope was limited to the effects of model parameter changes under singular angles and ideal weather conditions, without considering variables like climate or light changes and increased flight angles that deviate from ideal conditions in practical applications.

A preliminary classification of the LAI by fertility stage was conducted without a detailed examination of the varying impacts of LAI sizes on spectral reflectance. Besides the LAI, ALA emerges as a critical canopy structure parameter in the PROSAIL model [29], with sensitivity analyses indicating significant effects of Cab on spectral reflectance at specific wavelengths and ALA's influence exceeding 50% at certain wavelengths when LAI > 3. Therefore, acquiring precise canopy structure measurements and detailed spectral data is crucial for minimizing the impact of Cab and other parameters to refine LAI inversion accuracy. The RedEdge-P sensor contains only one band at the red-edge position, which presents a challenge in constructing a valid vegetation index. Future research should explore the extent of influence from variations in Cab data range and other canopy structure parameters on LAI inversion, aiming to optimize vegetation indices or model parameters to reduce their impact on LAI inversion outcomes and enhance overall accuracy.

4.3. Necessity of PROSAIL Model Parameter Calibration

During the whole growth cycle, the shoot of potatoes varies significantly. When retrieving the LAI for different growth stages or varieties, determining the model parameter ranges based on the measured data and prior knowledge can significantly improve the accuracy of LAI inversion [6]. Compared to the LAI retrieval method that uses only the reflectance of LAI-sensitive spectral bands, retrieving the LAI using the reflectance of five bands results in higher model accuracy. Therefore, multispectral sensors that capture more band information can be used to refine the data from each band, potentially further improving the accuracy of the inversion model.

4.4. Effect of Lookup Table Size on Model Results

The empirical modeling method of using the spectral vegetation index to invert crop physiological and biochemical parameters is severely limited due to the lack of physical principles and the small amount of radiation information [11]. The use of a radiative transfer model to invert vegetation parameters takes into account the optical characteristics of leaves and the radiative transfer characteristics of the canopy, which is a mechanistic method for vegetation parameter inversion [16]. LUT is a method of determining inversion parameters from a table driven by the distribution and co-distribution patterns of defined input variable sets and reflectance table sizes. The cost function was used to minimize the distance between the simulated reflectance and measured reflectance and then to determine

the entire set of primary input variables corresponding to the radiative transfer model based on LUTs [35]. At present, the lookup table size in the PROSAIL model is generally between 2500 and 100,000 [36]. Therefore, in order to compare the accuracy and computational efficiency of inverting the leaf area index with different lookup table sizes, this paper set five strategies ranging from 1000 to 50,000. The results show that when the lookup table size is 10,000, using the lookup table to invert the leaf area index has the best accuracy and the shortest calculation time. The density of numerical input for model parameters and the number of simulated spectra in the lookup tables significantly influence the inversion results [37]. Based on the sensitivity analysis, we constructed five lookup tables of different sizes to determine the optimal number of simulated spectra to include in the final lookup table; however, due to the large number of model parameters and the high density of model parameters, 10,000 simulated spectra had to be selected from over 10 million spectra using Latin hypercube sampling. Given the time constraints, only two types of LUTs were adopted in this study. Future research could focus on investigating the impact of lookup table size and the type of lookup tables on model accuracy. Efforts should also be made to mitigate the issue of poor model stability, which can arise from insufficient information in the lookup table and from a small number of lookup tables.

5. Conclusions

In this study, the ability of PROSAIL models combined with UAV multispectral imaging to estimate potato LAI at the plot scale was explored. The LAI has a significant influence on spectral reflectance. When the LAI is less than three, the contribution of potato LAI to the spectral reflectance in the visible light and red-edge bands ranges from 74.62% to 99.79%. The use of a lookup table containing 10,000 simulated spectra results in desirable model accuracy in a relatively short time. Based on the simulated spectral data, the LAI retrieval results using LUT1 for different growth stages and potato varieties demonstrated strong stability. The accuracy of the potato LAI retrieval model based on LUT2 was significantly higher than that of the LUT1, except during the tuber bulking stage.

The fusion of UAV multispectral imagery, the radiation transfer model, and machine learning algorithms significantly improves accuracy. Among the four inversion strategies tested, the hybrid model integrating UAV multispectral, PROSAIL, and PLSR yielded the most accurate and stable performance. Compared to the results obtained with LUT2, the hybrid model achieved higher accuracy, with the R^2 of the inversion model improving by 30% to 263%. Notably, the validation R^2 of the hybrid model combining PROSAIL and PLSR during the tuber bulking stage reached 0.87, which effectively overcame the low inversion accuracy observed with LUTs during the tuber bulking stage.

When compared with the empirical modeling method based on measured data, the hybrid method using simulated spectra also yielded good results for potato LAI retrieval. This suggests that PROSAIL has great potential for estimating potato LAI. Furthermore, the hybrid method can effectively reduce the challenges associated with constructing inversion models when sample sizes are insufficient or when measurement difficulties arise with larger numbers of plots. This approach presents a potential strategy for estimating potato LAI at the plot scale.

Author Contributions: Conceptualization, J.L. and S.L.; methodology, S.L.; formal analysis, S.L. and Y.L.; writing—original draft preparation, S.L. and J.L.; writing—review and editing, S.L., J.L., P.Z. and L.J.; supervision, J.L. and C.B.; funding acquisition, J.L. All authors have read and agreed to the published version of the manuscript.

Institutional Review Board Statement: Not applicable.

Data Availability Statement: Data will be made available upon request.

Conflicts of Interest: The authors declare no conflicts of interest.

Appendix A

Table A1. Parameterization of the PROSAIL model for sensitivity analysis.

Model	Abbr.	Variable	Unit	Data/Range (Local Sensitivity Analysis)	Data/Scope (Global Sensitivity Analysis)
PROSPECT-5	N	Leaf structure parameter	Unitless	1–2 (0.2), 1.5	1–2
	Cab	Chlorophyll a + b content	$\mu g \cdot cm^{-2}$	10–90 (10), 40	31–89
	Car	Carotenoids	$\mu g \cdot cm^{-2}$	2–14 (2), 5	6.3–14.1
	Cbrown	Brown pigments	$\mu g \cdot cm^{-2}$	0–1 (0.1), 0	-
	Cm	Dry matter content	$g \cdot cm^{-2}$	0.005–0.040 (0.005), 0.005	0.005–0.040
	Cw	Equivalent water thickness	$g \cdot cm^{-2}$	0.030–0.400 (0.01), 0.03	0.030–0.400
4SAIL	LAI	Leaf area index	$m^2 \cdot m^{-2}$	0–3 (0.5); 3–6 (0.5), 3.5	0–3; 3–6
	ALA	Average leaf inclination angle	°	36–65 (5), 50	36–65
	skyl	Diffuse/Direct light	Unitless	0–1 (0.2), 0.2	-
	psoil	Soil brightness coefficient	Unitless	0–1 (0.2), 0.2	-
	hspot	Hot spot	Unitless	0–1 (0.2), 0.33	0–1
	tts	Solar Zenith Angle	°	18.4–33.4 (3), 25	-
	tto	View Zenith Angle	°	0–90 (10), 0	-
	psi	Relative Azimuth Angle	°	0–90 (10), 0	-

Note: The data to the right of the sensitivity analysis column "," are the data used when setting fixed values; the data inside "()" are the step size when this parameter is a variable, e.g., LAI: 0–3 (0.5); 3–6 (0.5), 3.5. It is shown that when LAI is used as the variable to fix the other parameters, LAI is set in the ranges of 0–3 and 3–6, respectively, and local sensitivity analyses are performed in steps of 0.5.

Table A2. Constructing lookup table model parameter settings.

Model	Abbr.	Variable	Unit	M1	M2	Z5	D681	ALL
PROSPECT-5	N	Leaf structure parameter	Unitless	1–1.5 (0.1)	1–2 (0.1)	1–2 (0.1)	1–1.5 (0.1)	1–2 (0.1)
	Cab	Chlorophyll a + b content	$\mu g \cdot cm^{-2}$	55–88.1 (5)	31–76 (5)	31–83 (5)	33.7–88.1 (5)	31–88.1 (5)
	Car	Carotenoids	$\mu g \cdot cm^{-2}$	6–14.1 (0.5)	6.4–12.2 (0.5)	6–14.1 (0.5)	6–14.1 (0.5)	6.3–14.1 (0.5)
	Cbrown	Brown pigments	$\mu g \cdot cm^{-2}$	0	0	0	0	0
	Cm	Dry matter content	$g \cdot cm^{-2}$	0.004–0.037 (0.002)	0.008–0.05 (0.002)	0.004–0.032 (0.002)	0.004–0.05 (0.002)	0.004–0.05 (0.005)
	Cw	Equivalent water thickness	$g \cdot cm^{-2}$	0.03	0.03	0.03	0.03	0.03
4SAIL	LAI	Leaf area index	$m^2 \cdot m^{-2}$	0.3–2.4 (0.1)	0.6–5.5 (0.2)	0.3–3.5 (0.2)	0.3–5.5 (0.2)	0.3–5.5 (0.2)
	ALA	Average leaf inclination angle	°	57–60 (1)	60–65 (1)	57–65 (1)	57–65 (10)	57–65 (1)
	skyl	Diffuse/Direct light	Unitless	20	20	20	20	20

Table A2. *Cont.*

Model	Abbr.	Variable	Unit	M1	M2	Z5	D681	ALL
	psoil	Soil brightness coefficient	Unitless	0.2	0.2	0.2	0.2	0.2
	hspot	Hot spot	Unitless	0–1 (0.1)	0–1 (0.1)	0–1 (0.1)	0–1 (0.1)	0–1 (0.1)
	tts	Solar Zenith Angle	°	30	30	30	30	30
	tto	View Zenith Angle	°	0	0	0	0	0
	psi	Relative Azimuth Angle	°	0	0	0	0	0

Note: M1, M2, Z5, and ALL denote tuber initiation stage, tuber bulking stage, Zhongshu5, and full-life stage of the two varieties, respectively. The data in "()" are the parameter steps set when constructing the lookup table.

References

1. Devaux, A.; Goffart, J.-P.; Kromann, P.; Andrade-Piedra, J.; Polar, V.; Hareau, G. The potato of the future: Opportunities and challenges in sustainable agri-food systems. *Potato Res.* **2021**, *64*, 681–720. [CrossRef] [PubMed]
2. Watson, D. Comparative Physiological Studies on the Growth of Field Crops: II. The Effect of Varying Nutrient Supply on Net Assimilation Rate and Leaf Area. *Ann. Bot.* **1947**, *11*, 375–407. [CrossRef]
3. Begum, F.; Kundu, B.; Hossain, M. Physiological analysis of growth and yield of potato in relation to planting date. *J. Bangladesh Acad. Sci.* **2015**, *39*, 45–51. [CrossRef]
4. Xiao, Z.; Liang, S.; Wang, J.; Xiang, Y.; Zhao, X.; Song, J. Long-Time-Series Global Land Surface Satellite Leaf Area Index Product Derived from MODIS and AVHRR Surface Reflectance. *IEEE Trans. Geosci. Remote Sens.* **2016**, *54*, 5301–5318. [CrossRef]
5. Allen, W.; Richardson, A. Interaction of Light with a Plant Canopy. *J. Opt. Soc. Am.* **1968**, *58*, 1023–1028. [CrossRef]
6. Nathalie, B. Ground-based measurements of leaf area index: A review of methods, instruments and current controversies. *J. Exp. Bot.* **2003**, *54*, 2403–2417.
7. Wilson, J.W. Estimation of foliage dense-ness and foliage angle by inclined point quadrats. *Aust. J. Bot.* **1963**, *11*, 95–105. [CrossRef]
8. Impollonia, G.; Croci, M.; Blandinières, H.; Marcone, A.; Amaducci, S. Comparison of PROSAIL Model Inversion Methods for Estimating Leaf Chlorophyll Content and LAI Using UAV Imagery for Hemp Phenotyping. *Remote Sens.* **2022**, *14*, 5801. [CrossRef]
9. Roosjen, P.; Brede, B.; Suomalainen, J.; Bartholomeus, H.; Kooistra, L.; Clevers, J. Improved estimation of leaf area index and leaf chlorophyll content of a potato crop using multi-angle spectral data—Potential of unmanned aerial vehicle imagery. *Int. J. Appl. Earth Obs. Geoinf.* **2018**, *66*, 14–26. [CrossRef]
10. Yu, T.; Zhou, J.; Fan, J.; Wang, Y.; Zhang, Z. Potato Leaf Area Index Estimation Using Multi-Sensor Unmanned Aerial Vehicle (UAV) Imagery and Machine Learning. *Remote Sens.* **2023**, *15*, 4108. [CrossRef]
11. Berger, K.; Atzberger, C.; Danner, M.; D'Urso, G.; Mauser, W.; Vuolo, F.; Hank, T. Evaluation of the PROSAIL Model Capabilities for Future Hyperspectral Model Environments: A Review Study. *Remote Sens.* **2018**, *10*, 85. [CrossRef]
12. Gustau, C.; Dino, S.; Jakob, R.; Markus, R. A perspective on Gaussian processes for Earth observation. *Natl. Sci. Rev.* **2019**, *6*, 616–618.
13. Su, W.; Wu, J.; Wang, X.; Xie, Z.; Zhang, Y.; Tao, W.; Jin, T. Retrieving Corn Canopy Leaf Area Index Based on Sentinel-2 Image and PROSAIL Model Parameter Calibration. *Spectrosc. Spectr. Anal.* **2021**, *41*, 1891–1897.
14. Sun, J.; Wang, L.; Shi, S.; Li, Z.; Yang, J.; Gong, W.; Wang, S.; Tagesson, T. Leaf pigment retrieval using the PROSAIL model: Influence of uncertainty in prior canopy-structure information. *Crop J.* **2022**, *10*, 1251–1263. [CrossRef]
15. Sun, Y.; Wang, B.; Zhang, Z. Improving Leaf Area Index Estimation with Chlorophyll Insensitive Multispectral Red-Edge Vegetation Indices. *IEEE J. Sel. Top. Appl. Earth Obs. Remote Sens.* **2023**, *16*, 3568–3582. [CrossRef]
16. Zhang, C.; Liu, X.; Wang, R.; Wei, N.; Liu, J.; Yu, K.; Wang, F. A Study on Canopy Water Content Inversion of *Phyllostachys edulis* Forest Based on PROSAIL Model. *J. Northwest For. Univ.* **2023**, *38*, 224–232+249.
17. Wang, R.; Chen, J.M.; He, L.; Liu, J.; Shang, J.; Liu, J.; Dong, T. A novel semi-empirical model for crop leaf area index retrieval using SAR co- and cross-polarizations. *Remote Sens. Environ.* **2023**, *296*, 113727. [CrossRef]
18. David, H.; Urte, S.; Andreas, W. Machine Learning Techniques for Predicting Crop Photosynthetic Capacity from Leaf Reflectance Spectra. *Mol. Plant* **2017**, *10*, 878–890.
19. Houborg, R.; Anderson, C. Utility of an image-based canopy reflectance modeling tool for remote estimation of LAI and leaf chlorophyll content at regional scales. *J. Appl. Remote Sens.* **2009**, *3*, 033529.
20. Elizabeth, B.; Brigitte, L.; Bernie, Z.; James, W. Non-destructive estimation of potato leaf chlorophyll from canopy hyperspectral reflectance using the inverted PROSAIL model. *Int. J. Appl. Earth Obs. Geoinf.* **2007**, *9*, 360–374.
21. Su, W.; Sun, Z.; Chen, W.-H.; Zhang, X.; Yao, C.; Wu, J.; Huang, J.; Zhu, D. Joint Retrieval of Growing Season Corn Canopy LAI and Leaf Chlorophyll Content by Fusing Sentinel-2 and MODIS Images. *Remote Sens.* **2019**, *11*, 2409. [CrossRef]

22. Duan, S.; Li, Z.; Wu, H.; Tang, B.; Ma, L.; Zhao, E.; Li, C. Inversion of the PROSAIL model to estimate leaf area index of maize, potato, and sunflower fields from unmanned aerial vehicle hyperspectral data. *Int. J. Appl. Earth Obs. Geoinf.* **2014**, *26*, 12–20. [CrossRef]

23. Luo, W.; Li, R.; Shen, F.; Liu, J. HY-1C/D CZI Image Atmospheric Correction and Quantifying Suspended Particulate Matter. *Remote Sens.* **2023**, *15*, 386. [CrossRef]

24. Zhang, M.; Su, W.; Zhu, D. Retrieval of LAI and LCC in Summer Corn Canopy Based on the PROSAIL Model Using an Improved Inversion Strategy. *Geogr. Geo-Inf. Sci.* **2019**, *35*, 28–33.

25. Jin, X.; Diao, W.; Xiao, C.; Wang, F.; Chen, B.; Wang, K.; Li, S. Estimation of Wheat Agronomic Parameters using New Spectral Indices. *PLoS ONE* **2013**, *8*, e72736. [CrossRef]

26. Zhen, Z.; Chen, S.; Yin, T.; Chavanon, E.; Lauret, N.; Guilleux, J.; Henke, M.; Qin, W.; Cao, L.; Li, J.; et al. Using the Negative Soil Adjustment Factor of Soil Adjusted Vegetation Index (SAVI) to Resist Saturation Effects and Estimate Leaf Area Index (LAI) in Dense Vegetation Areas. *Sensors* **2021**, *21*, 2015. [CrossRef]

27. Qiao, K.; Zhu, W.; Xie, Z.; Li, P. Estimating the Seasonal Dynamics of the Leaf Area Index Using Piecewise LAI-VI Relationships Based on Phenophases. *Remote Sens.* **2019**, *11*, 689. [CrossRef]

28. Xie, Q.; Huang, W.; Liang, D.; Chen, P.; Wu, C.; Yang, G.; Zhang, D. Leaf Area Index Estimation Using Vegetation Indices Derived from Airborne Hyperspectral Images in Winter Wheat. *IEEE J. Sel. Top. Appl. Earth Obs. Remote Sens.* **2014**, *7*, 3586–3594. [CrossRef]

29. Jiao, Q.; Sun, Q.; Zhang, B.; Huang, W.; Ye, H.; Zhang, Z.; Zhang, X.; Qian, B. A Random Forest Algorithm for Retrieving Canopy Chlorophyll Content of Wheat and Soybean Trained with PROSAIL Simulations Using Adjusted Average Leaf Angle. *Remote Sens.* **2022**, *14*, 98. [CrossRef]

30. Wold, S.; Sjöström, M.; Eriksson, L. PLS-regression: A basic tool of chemometrics. *Chemom. Intell. Lab. Syst.* **2001**, *58*, 109–130. [CrossRef]

31. Mutanga, O.; Masenyama, A.; Sibanda, M. Spectral saturation in the remote sensing of high-density vegetation traits: A systematic review of progress, challenges, and prospects. *ISPRS J. Photogramm. Remote Sens.* **2023**, *198*, 297–309. [CrossRef]

32. Li, W.; Weiss, M.; Waldner, F.; Defourny, P.; Demarez, V.; Morin, D.; Hagolle, O.; Baret, F. A Generic Algorithm to Estimate LAI FAPAR and FCOVER Variables from SPOT4 HRVIR and Landsat Sensors: Evaluation of the Consistency and Comparison with Ground Measurements. *Remote Sens.* **2015**, *7*, 15494–15516. [CrossRef]

33. Danner, M.; Berger, K.; Wocher, M.; Mauser, W.; Hank, T. Fitted PROSAIL Parameterization of Leaf Inclinations, Water Content and Brown Pigment Content for Winter Wheat and Maize Canopies. *Remote Sens.* **2019**, *11*, 1150. [CrossRef]

34. Xu, Z.; He, A.; Zhang, Y.; Hao, Z.; Li, Y.; Xiang, S.; Li, B.; Chen, L.; Yu, H.; Shen, W.; et al. Retrieving chlorophyll content and equivalent water thickness of Moso bamboo (*Phyllostachys pubescens*) forests under *Pantana phyllostachysae* Chao-induced stress from Sentinel-2A/B images in a multiple LUTs-based PROSAIL framework. *For. Ecosyst.* **2023**, *10*, 100108. [CrossRef]

35. Weiss, M.; Frédéric, B.; Myneni, B.; Agnès, P.; Knyazikhin, Y. Investigation of a model inversion technique to estimate canopy biophysical variables from spectral and directional reflectance data. *Agronomie* **2000**, *20*, 3–22. [CrossRef]

36. He, W.; Yang, H.; Pan, J.; Xu, P. Exploring optimal design of look-up table for prosail model inversion with multi-angle modis data. *Proc. SPIE Int. Soc. Opt. Eng.* **2012**, *8524*, 852420.

37. Wang, Z.; Skidmore, A.K.; Wang, T.; Darvishzadeh, R.; Hearne, J. Applicability of the PROSPECT model for estimating protein and cellulose plus lignin in fresh leaves. *Remote Sens. Environ.* **2015**, *168*, 205–218. [CrossRef]